Journal of Thermal Analysis, Vol. 37 (1991) 1065-1101

Special Review

PHOTOTHERMAL APPLICATIONS TO THE THERMAL ANALYSIS OF SOLIDS

A. Mandelis

PHOTOACOUSTIC AND PHOTOTHERMAL SCIENCES LABORATORY,DEPARTMENT OF MECHANICAL ENGINEERING, UNIVERSITY OF TORONTO, TORONTO, ON, M5S 1A4, CANADA

(Received April 29, 1991)

Major application of optically-induced thermal waves to the thermal and thermodynamic analysis of solids are reviewed. The spectrum of available techniques,from the conventional photoacoustic detection to novel photothermal laser probing and frequency multiplexing is discussed, and their utilization for the measurement of thermophysical thermal transport-related parameters of solids is presented. These include the thermal diffusivity, effusivity, conductivity and specific heat. The ability of photothermal methods to perform thermal analysis on large classes of solids, including conducting and insulating bulk materials, crystals, layered porous and coated structures, thin films and inhomogeneous thermal profiles is highlighted. Finally, special capabilities of photothermal analysis, such as the monitoring of surface thermodynamic phenomena and phase transition studies, including high-T_c superconductors, are described in order to give a complete overview of the rich potential of photothermal-based methodologies.

Exposure of a sample to radiation results in local heating due to absorption and subsequent thermalization of the incident radiation. The extent of absorption and the thermalized volume fraction depend on the interplay between the absorption profile and the thermal transport properties of the material under investigation. If the irradiance of the incident radiation is modulated harmonically or pulsed, an oscillatory or transient heat source, respectively, is generated in the sample. Thermal waves are thus created,

John Wiley & Sons, Limited, Chichester
Akadémiai Kiadó, Budapest

which interact with the sample before being detected is one of several available photothermal sensing methods.[1–4] Due to thermal expansion acoustic waves are simultaneously launched into the sample and their detection is the object of various photoacoustic detection schemes, primarily through the intimate contact of the sample with an acoustic piezoelectric transducer.[5, 6] These photoacoustic phenomena are outside the scope of this review, with the exception of the conventional microphonic photoacoustic (PA) detection [7] which, in several applications important to thermal analysis, uses acoustic waves primarily assimple, passive carriers of thermal-wave signals to a remote microphone for detection. Depending on the physical principle(s) on which the thermal-wave sensor is operating, important photothermal (PT) schemes for thermal analysis to-date, besides PA detection, are laser beam deflection (or Mirage effect), photothermal radiometry, photopyroelectric detection, and laser-surface interaction based methods. These techniques are ideal for the thermal analysis of broad classes of matter, including fluids and gases. In this review, we will only examine solid phase applications. Although thermal waves may be generated in a sample through the incidence and nonradiative conversions of either modulated or pulsed optical energy, or even with electrons, ions or neutral particles, the great majority of thermal analyses has been performed with optical photon sources. Furthermore, depending on the mode of signal generation and detection, photothermal instrumentation schemes can be divided into synchronous (frequency-domain, FD), transient (time-domain, TD) and intermediate frequency-multiplexed (FM).

In Section I a brief overview of the PA methodology and selected applications to thermal analysis will be presented, followed, by PT methodologies, such as Mirage effect, Photothermal Radiometry and Photopyroelectric detection and applications to wide ranges of solids in Section II. Section III is a discussion of non-conventional photothermal application to thermal analysis, including phase transitions and laser-surface thermal interactions. These perspectives are aimed to indicate the potential of photothermal detection schemes and the role they are likely to play in the evolution of the field of Thermal Analysis.

I. Photoacoustic methodologies

a) General configuration

A generic thermal-wave production instrumentation scheme is shown in Fig. 1. The light source consists of either a broadband lamp (e.g. 1000 W Xe lamp) or a laser.[2] The collimated output photon beam is modulated by a mechanical chopper for FD measurements, or an acousto-optic (AO) or electro-optic modulator for high-frequency FD and FM measurements. For TD measurements a pulsed laser source is used. A beam splitter is inserted in the path of the optical beam, re-directing part of the optical power to a reference sample or a power meter, A, which is used to yield a reference signal proportional to the incident power on the sample. The output signal B from the sample when normalized in the form B/A is compensated with respect to the photon counts, optical beam fluctuations and for the transfer function of the PT detector and detection electronics. The physical principle on which the PT transducer operates gives the technique its name. For purposes of thermal analysis-related measurements, it is generally desirable to use a single output wavelength from the source in such a spectral region that the sample (or part thereof) is optically opaque, i.e. the optical penetration depth is very small compared to the shortest thermal diffusion length, $\mu_s(f)$, a function of modulation frequency, in the sample. In the frequency domain this condition can be written[7]

$$\beta^{-1} << \mu_s(f) \equiv \left[\frac{\pi f}{\alpha_s}\right]^{1/2} \tag{1}$$

where $\beta(\lambda)$ is the optical absorption coefficient of the sample at wavelength λ; f is the optical beam modulation frequency, and α_s is the (assumed homogenous) sample thermal diffusivity. In this limit, the resulting photothermal signal can be shown to be independent of $\beta(\lambda)$, and dependent only on geometrical and sample thermal parameters, [7–10] a condition known as *photothermal saturation*. Time-domain conditions equivalent to (1) have also been presented. As an example, the temporal regime of PA saturation following a single laser pulse was found to be [11]

$$t >> \tau_\beta \equiv \frac{1}{\beta^2}\,\alpha_s \tag{2}$$

for uniform surface illumination of semi-infinite and laterally infinite samples, an easy experimental condition to attain. A simple method for

satisfying conditions of photothermal saturation for a given example is by depositing a thin black coating on its surface, so that the optical-to-thermal energy conversion acts as a surface and all subsequent signal evolution is independent of optical absorption and optically suitable for thermal analysis studies.

b) FD photoacoustic detection

With this detection mode, the transducer in Fig. 1 is (usually) a condenser or electret microphone and the sample is placed in a hermetically sealed container of minimal volume (i.e. small compared to the acoustic wavelength with transparent window, allowing the incident radiation of irradiance I_o to penetrate the acoustic chamber and impinge on the sample

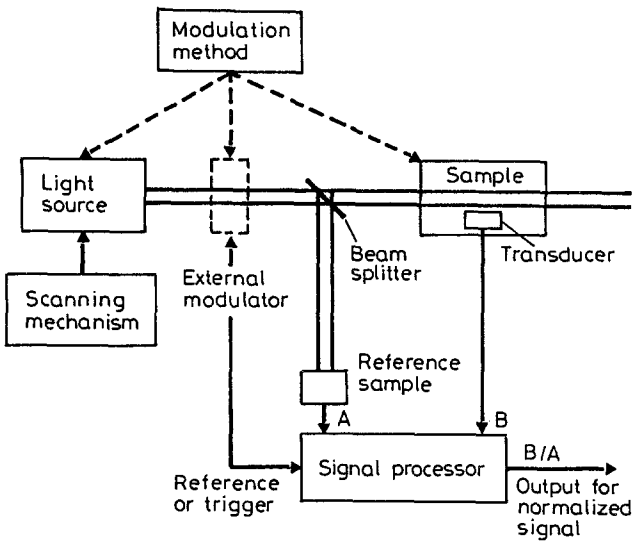

Fig. 1 Generic photothermal instrumentation, including FD, TD and FM detection schemes

surface. The intensity of the radiation is assumed to be modulated with a mechanical chopper or an AO modulator with a time dependence given by

$$I(t) = \frac{1}{2} I_0 (1 + \cos \omega t) \qquad \left[\frac{\mathrm{W}}{\mathrm{m}^2}\right] \tag{3}$$

and the distributed thermal-wave source generated at depth z following absorption and non-radiative energy conversion has a density

$$Q(\beta,\omega) = \frac{1}{2}\beta I_0 e^{-\beta|x|}(1+\cos\omega t) \qquad \left[\frac{W}{m^3}\right] \tag{4}$$

The optical intensity modulation has been shown [12] to result in a periodic temperature variation within a gas boundary layer above the sample. The gas of choice is usually air and the mean temperature of the boundary layer, which extends over one thermal diffusion length $\mu_g(f)$ in the gas, is given by [7]

$$\bar{T}(t) = (\theta/2\pi\sqrt{2})\exp[i(\omega t - \pi/4)] \tag{5}$$

where θ is the complex temperature envelope, which involves the thermal transport properties of the sample. The thermal wave thus generated produces an alternating pressure disturbance, acting as an adiabatic piston on the rest of the gas column beyond the boundary layer. In order to minimize acoustic noise and maximize the signal-to-noise ratio (SNR), a microphone preamplifier and a lock-in amplifier are used as signal processor units, Fig. 1. Lock-in detection takes place at audio frequencies outside the band of the acoustic noise spectrum of the environment. The amplitude and phase lag to the PA signal can then be stored in a computer and displayed.

The experimental setup described above can be used straightforwardly in thermal analysis of solids to measure thermal diffusivity. Early work by Adams and Kirkbright [13] demonstrated quantity. Those authors used a transparent sample model of thickness d with an opaque underlayer and showed that the PA signal theory is significantly simplified [14]

$$S(\omega) = S_0 \exp[-d/\mu_s(\omega)] \qquad \text{(amplitude)} \tag{6a}$$

$$\Delta\Phi(\omega) = d/\mu_s(\omega) \quad \text{(phase lag)} \tag{6b}$$

In Eq. (6) $\mu_s(\omega)$ is given by Eq. (1) with $\omega = 2\pi f$. Experimentally, they used a thin glass coverslip of known thickness, one face of which was coated with black enamel. The PA signal phase, using a 1000 W Xe lamp (white light), was recorded as a function of frequency f and the thermal diffusivity of the glass cover-slip was calculated from the slope G of the straight line obtained and the expression

$$\alpha_s = d^2/2G^2 = 9.8 \pm 0.5 \cdot 10^{-3} \qquad \text{cm}^2/\text{s} \tag{7}$$

where Eq. (6b) was used and $G = \mathrm{d}(\Delta\Phi)/\mathrm{d}(\sqrt{\omega})$. The value of α_s thus calculated was found to be in reasonable agreement with literature values for glass. The method illustrates the simplicity of PA thermal analysis for specific types of solids.

Depending on the relationship between the sample thickness, l_s, and the thermal diffusion length, $\mu_s(f)$, the saturated PA signal can also yield meausrements of the thermal effusivity. This is the case if $l_s > \mu_s > \beta^{-1}$. In this limit the sample generated signal ratio to that of a reference sample is [7]

$$\frac{S_s(\omega)}{S_{ref}(\omega)} = \frac{e_s}{e_{\mathrm{ref}}}, \tag{8}$$

where

$$e_s = (\rho_s\, c_s\, k_s)^{1/2} \tag{9}$$

is the thermal effusivity of a solid with density ρ_s, specific heat c_s, and thermal conductivity k_s. Lyamov *et al.* [15] used this result to determine the effusivities of single superconducting crystals of Ge, Si, and CdSe and obtained data in the 39 Hz–1275 Hz regime. Their results were Ge, Si, and CdSe and obtained data in the 39 Hz–1275 Hz regime. Their results were

$$S_{\mathrm{CdSe}} / S_{\mathrm{Ge}} = 5.54 \pm 0.81 \quad (5.4)$$

$$S_{\mathrm{CdSe}} / S_{\mathrm{Si}} = 6.86 \pm 1.17 \quad (7.14)$$

$$S_{\mathrm{Ge}} / S_{\mathrm{Si}} = 1.24 \pm 0.14 \quad (1.32)$$

with tabulated literature values in parentheses. Knowledge of a reference e_{ref} value can give good estimations of the thermal effusivity of solids using PA detection. Care must be taken however with respect to the validity of the relation $l_s > \mu_s$; otherwise contributions from the thermal effusivity of the backing material, e_b, can introduce large errors in the relative or absolute measurement of e_s. The saturated PA signal in this case can be written as[16]:

$$S(\omega) = \frac{S_0}{k_s \alpha_s^{1/2} x^2}\left[\frac{1 + R^2 e^{-4x} + 2Re^{-2x}\cos 2x}{[(1 - R^2 e^{-4x})^2 + 4R^2 e^{-4x}\sin^2 2x]^{1/2}}\right] \quad \text{(amplitude)} \tag{10a}$$

and

$$\Delta\Phi = \tan^{-1}\left[\frac{2R\sin 2x}{e^{2x} - R^2 e^{-2x}}\right] \qquad \text{(phase)} \tag{10b}$$

where S_0 is constant independent of material thermal properties; R is an interfacial thermal-wave reflection coefficient

$$R = (1-b)/(1+b); \quad b \equiv \frac{e_b}{e_s} \tag{11}$$

and

$$x = (f/f_c)^{1/2} \tag{12}$$

with f_c a 'critical' chopping frequency, at which the thermal diffusion length in the sample is equal to its thickness:

$$\mu_s(f_c) = l_s \rightarrow f_c = \alpha_s/\pi l_s^2 \tag{13}$$

Madhusoodanan *et al.* [17] used the PA signal dependence on thermal effusivities e_s and e_b coupled through the further relationships

$$\alpha_s = k_s/\rho_s c_s \tag{14}$$

and

$$e_s = k_s\sqrt{\alpha_s} \tag{15}$$

in order to measure α_s, k_s, and e_s of several polymers supported in a PA cell by backings of known thermal properties (water and benzene}. Their results are shown in Table 1. It should be noted that in order to calculate the quantities shown in Table 1 from the PA phases, reference samples were used and the PA phases of the samples were subtracted from that of the reference to obtain $\delta\Phi$, Eq. (10b). As a result of PA measurements of uniform solids with the help of calibration curves from reference samples, the FD–PA technique can provide complete information on thermal diffusivity (primary quantity), conductivity and effusivity (derivative quantities from Eqs (14) and (15)). Extensive use of the conventional PA detection method for the study of technical graphite materials used in Tokamak devices has been made at Ruhr University. A high-temperature photoacoustic cell was built [18] for operation up to 1000 K and the thermal diffusivity of graphite samples of thickness between 1 mm and 1.9 mm has been measured absolutely using no signals from samples of different thicknesses, with no need for a reference

Table 1 The thermal parameters of several polymers with water as a backing material, with $e_b = 3.8 \cdot 10^{-2}$ cal $\cdot$ cm$^{-2} \cdot$ K$^{-1} \cdot$ s$^{-1/2}$ [From Ref. 17]

Material	Thickness,	Method used							
		Amplitude measurement				Phase measurement			
		f_c,	α_s,	k_s,	e_s,	f_c,	α_s,	k_s,	e_s,
	μm	Hz	$\cdot 10^{-4}$ cm$^2 \cdot$ s^{-1}	$\cdot 10^{-4}$ cal/cm s °C	$\cdot 10^{-2}$ cal cm^{-2} K^{-1} s$^{-1/2}$	Hz	$\cdot 10^{-3}$ cm$^2 \cdot$ s^{-1}	$\cdot 10^{-4}$ cal/cm s °C	$\cdot 10^{-2}$ cal cm^{-2} K^{-1} s$^{-1/2}$
Cellulose acetate	30	115	1.04	5.20	1.62	120	1.08	5.40-	1.64
Teflon	25	182	1.14	6.08	1.80	178	1.11	5.95	1.78
Polystyrene	30	91	0.82	2.78	0.97	97	0.87	2.80	0.95
Polyacetal	35	112	1.37	6.80	1.84	105	1.29	6.40	1.78

material. Then the effusivity of the graphite bulk material was determined using molybdenum samples as a reference. It is interesting to note that the frequency dependence of the PA signals at various ambient temperatures from 300–1000 K was monitored to assess the character of the effusivity depth profile: departures of the frequency dependence expected from uniform, homogenous materials is an indication of varying thermal parameters and photothermal detection can be used to study such variations, as discussed below. Bein and Pelzl [19] used Eq. (8) applied to the surface temperatures of a rough and a smooth solid to calculate the effective effusivity, e_r, of rough graphite, using a roughness model based on the concept of surface porosity. These considerations were further used to qualitatively study effusivity depth profiles of graphite plates before and after exposure to the Tokamak plasma: [20] lattice damage due to energetic particle bombardment (ions, charge-exchange neutrals) was found to dominate thermal behavior of relatively cool graphite regions. Possible changes in microporosity were assumed to be responsible for the behavior of sample regions heated during incorporation in the Tokamak device.

PA models for multi-layered solids have been advanced by Mandelis *et al.* [21] and Fernelius [22]. The former theory for bilayered samples with distinct thermal (as well as optical) properties has been applied to thermal studies on ion implanted semiconductors [23, 24]: in such materials, thermal and optical parameter degradation within the implanted region is observed and photothermal analysis provides a unique tool for their measurement. A further success of PA detection using the bilayered model [21] was in the study of biporous fuel cell nickel electrodes fabricated with substantially different void fractions. Mandelis and Lymer [25] used irradiation from a He–Ne laser and showed that such electrodes behaved photoacoustically like solids made of two homogeneous and continuous layers, if the porosity range were ~40–80%. Using the bilayered model (which is valid only for continuous layers) they also calculated mean thermal diffusivities and conductivities for each layer by fitting the frequency response data to the expression for the PA signal for the photoacoustically saturated bilayer:

$$T_s(0,\omega) = \left[\frac{I_0}{2k_1\sigma_1}\right][(b_1+1)(b_2+1)\exp(\sigma_1 L_1+\sigma_2 L_2)$$

$$+(b_1-1)(b_2-1)\exp(\sigma_1 L_1-\sigma_2 L_2)-(b_1+1)(b_2-1)\exp(-\sigma_1 L_1-\sigma_2 L_2)$$

$$-(b_1-1)(b_2+1)\exp(-\sigma_1 L_1+\sigma_2 L_2)]$$

$$[(b_1+1)(b_2+1)\exp(\sigma_1 L_1+\sigma_2 L_2)+(b_1-1)(b_2+1)\exp(-\sigma_1 L_1+\sigma_2 L_2)$$

$$+(b_1+1)(b_2-1)\exp(-\sigma_1 L_1-\sigma_2 L_2)+(b_1-1)(b_2-1)\exp(-\sigma_1 L_1-\sigma_2 L_2)] \quad (16)$$

where I_o is the incident light intensity (W/cm^2) assumed spatially uniform, L_1 and L_2 are the layer thicknesses, and

$$\sigma_j \equiv (1+i)(\omega/2a_j)^{1/2}; \qquad j=1,2$$

$$b_1 \equiv k_2\sqrt{a_1}/k_1\sqrt{a_2}$$

and

$$b_2 \equiv k_b\sqrt{a_2}/k_2\sqrt{a_b}$$

k_j is the thermal conductivity of material (j); $j=1, 2, b$. The backing material (b) for the experiments in this work was aluminium, whose thermal properties are: $a_{Al}=0.82\ cm^2/s$, $k_{Al}=2.01\ W/cm\cdot K$. Solid layer 1 was identified with the coarse-pore layer, and solid layer 2 with the fine-pore layer.

Figure 2 shows these fits and the calculated thermal quantities. The trend in these quantities is in general agreement with thermal analysis trends obtained for MgO, Al_2O_3 and ZrO_2 powders of variable (controlled) pore sizes with the added advantage of considerable experimental system simplicity compared to the quite complicated setup for conventional thermal conductivity measurements used in those studies. Their method further lacks the ability to simultaneously provide a value for the diffusivity of the sample. Bein *et al.* [27] recently used a multilayered sample model to address porosity-porous bulk problem encountered with graphite or ceramic materials used in Tokamaks. They were also able to obtain information about the diffusivity and effusivity of subsurface regions, irrespective of the effect of the inherent surface roughness. In a variant of the above PA methodology, Aithal *et al.* [28] used scanning of an A1 sample (3 mm thick) with a Teflon defect embedded in a 108 μm-thick coating on Al, as well as other metallic substrates with metallic plasma-sprayed coatings. By studying the PA phase and amplitude variations with the pump laser beam modulation frequency and using a method adapted from conventional PA thermal analysis[29, 30], those authors were able to determine the coating (Ni–Cr–6% Al alloy; and aluminium) effusivity and diffusivity coefficients. A frequency variation study of the PA signal in the Teflon defect region gave

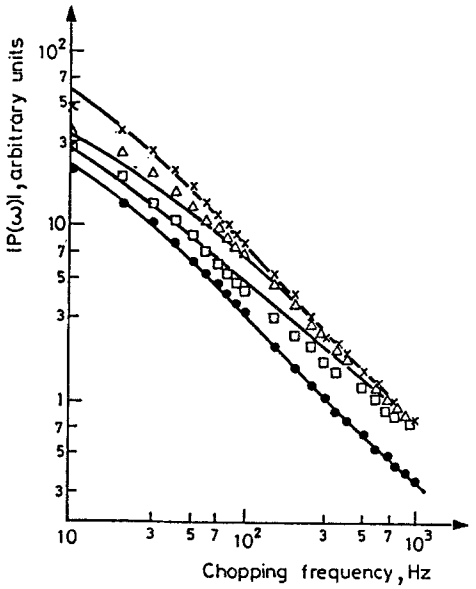

Fig. 2 Least-squares fit of PA amplitude frequency response, to the model of Eqs (16). Coarse-pore layer thickness L_1: *A*, (-x-x-) 200 μm; *B*, (-Δ-Δ-) 76 μm; *C*, (-□-□-) 25 μm; *D*, (-•-•-) 13 μm. Fine pore layer thickness $L_2 = 0.56$ mm

Table 2 Thermal properties of materials used as defects and coatings (a) Tabulated values are from Y.S. Touloukian, *Thermophysical Properties of Matter*, Vols 1,2,10, IFI-Plenum, New York, 1970. [from Ref. 28]

Material	Conductivity, K	Diffusivity, α	Experimental effusivity, $K\alpha^{-1/2}$	Experimental diffusivity, α	Deduced conductivity, K
	$Wm^{-1}K^{-1}$	m^2s^{-1}	$JK^{-1}s^{-1/2}m^{-2}$	m^2s^{-1}	$Wm^{-1}K^{-1}$
Teflon	0.4	$1.2 \cdot 10^{-7}$			
Alumina	30	$7.5 \cdot 10^{-7}$			
Ni–Cr–6% Al	11	$3.4 \cdot 10^{-6}$	$3.7 \cdot 10^{3}$	$3.6 \cdot 10^{-6}$	7
Aluminium	234	$9.7 \cdot 10^{-5}$	$2.5 \cdot 10^{4}$	$8.4 \cdot 10^{-5}$	230

its thermal resistence R as $2 \cdot 10^{-5}\ m^2 \cdot K \cdot W^{-1}$. Table 2 shows some of these results.

c) Alternate FD photoacoustic detection schemes

In addition to the conventional PA technique applied to thermal analysis, a few alternate schemes have been used. Rear surface illumination if schematically juxtaposed to front surface illumination in Fig. 3. In that geometry, the photoacoustically saturated, thermally thick regime [7] (i.e.$l_s >> \mu_s(f)$)signal is given by the very simple expression. [31]:

$$S_R(f) = \frac{K_R}{f} \exp\left[- \left(\frac{\pi f}{\alpha_s}\right)^{1/2} l_s \right] \tag{17}$$

where K_R is a frequency-independent constant. The slope of the $ln\ (S_R f)$ *vs.* $f^{1/2}$ plot can give the thermal diffusivity of a sample under rear surface illumination. The technique has been used [31] to calculate α_s of benzophenone at several background temperatures in the range 118 K–293 K. Although no literature thermal data existed for benzophenone, other than its room temperature value, $1.8 \cdot 10^{-3}$ cm^2/s, the authors found reasonable agreement with the temperature-dependent diffusivity values reported in the literature for other organic solids. In a thorough rear surface illumination study of thin copper film (40–60 μm thickness range), Hashimoto *et al.* [32] measured the diffusivity of the thin films, while at the same time they observed a sound wave interference effect in the PA cell. This effect causes an extra phase lag between the modulated light and the microphone signal and seems to complicate the measurements of thin films by PA detection. Other photothermal methods not based on acoustic detection have proven to be simpler and more straightforward for thin-film thermal analysis, as will be

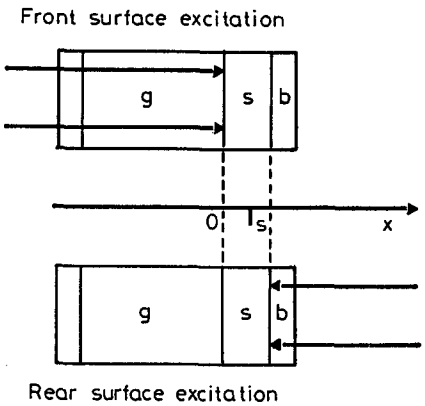

Fig. 3 Principle of the front and rear PA detection schemes; b: backing, s: sample, g: gas [from Ref. 31]

discussed farther on. Nevertheless, Korpiun *et al.* [33] performed PA rear-surface measurements of the absolute values of the diffusivity of commercial polyethylenterephthalate (PETP) foils of 19 μm thickness as received from the manufacturer, as well as of relative changes in the thermal diffusivity by uniaxially drawing these foils in two different directions. Figure 4 shows these relative changes; such variations in diffusivity upon drawing down to 1% could be determined with higher accuracy than absolute values and are consistent with the aggregate model of Kilian and Pietralla[34] or the two-phase model of Choy and Young [35]. In a variant of the rear-surface illumination geometry of Fig. 3, Perondi and Miranda [36] minimized the PA cell volume, an optimization required by the reciprocal relationship between the acoustic pressure wave and the gas volume. This was done by placing the sample directly on top of the PA cell's condenser microphone surface, which has a 2 mm diameter hole, with a minimal gas volume (1 mm-high) between the front sound inlet and the active diaphragm. As a result, the thermal diffusivity of several solids was easily determined from the PA signal frequency

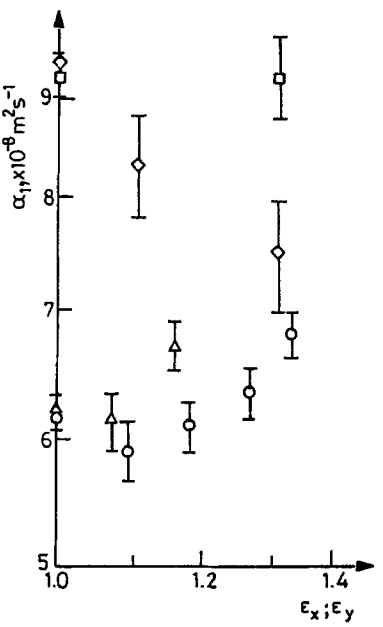

Fig. 4 Thermal diffusivity of PETP foils in z-direction *vs.* draw ratio. '19 μm' foils drawn in x-direction (□) and y-direction (◇); '30 μm' foils drawn in x-direction (○) and y-direction (△). ε_i is referred to the initial draw ratios ε_x^0 and ε_y^0 set equal to one [from Ref. 33]

response in the thermally thin regime [7], (i.e. $l_s << \mu_s(f)$) as in Eq. (15). At higher frequency measurements (thermally thick samples), a frequency dependence $\sim f^{-1}$, instead of the expected exponential behavior, suggested that thermoelastic bending of the sample is the dominant mechanism responsible for the PA signal, as previously demonstrated by Rousset *et al.* [37]. Good agreement of diffusivity values with literature data was reported (see Table 3). Charpentier *et al.* [29] also used rear-surface illumination in the sense of Fig. 3 and measured the thermal diffusivity and thermal expansion coefficient of several metals (Al, Zn, Fe, Cu). The latter parameter is only measurable with rear-surface illumination, due to the sample periodic thermal expansion, which is coherent with the optical excitation and is referred to as the 'acoustic pistol' effect. Thermal diffusivity measurements with this

Table 3 Comparison of the thermal diffusivity values from the open PA cell technique with the values quoted in the literature [from Ref. 36]

Material	Measured, cm^2/s	Literature values, cm^2/s
Aluminium	0.99	0.94
Silicon	0.87	0.85
Low-density polyethylene	0.0017	0.0016
High-density polyethylene	0.0020	0.0022
Polypropylene	0.0011	0.0009

geometry must be performed with thermally thick samples, in order to avoid the acoustic piston and the 'drum' effect (due to the periodic dilatation) of the sample. For this reason careful fixing of the sample on the backing is needed.

An alternate PA technique well suited for thermal analysis without the experimental pitfalls of the conventional rear-surface illumination methods is a combination of front and back techniques, introduced by Pessoa *et al.* [38] and shown in Fig. 5. Using the thermal diffusion model of Rosencwaig and Gersho [7] for the production of the PA signal, the ratio S_F/S_R of the signal amplitude and phase difference, $\Delta\Phi = \Phi_F - \Phi_R$, for front ($F$) and rear ($R$)-surface illumination are given by [38]

$$S_F/S_R = \left(I_F/I_R\right) \left| \cosh^2\left(l_s/\mu_s\right) - \sin^2\left(l_s/\mu_s\right) \right|^{1/2} \qquad (18a)$$

and

$$\tan\left(\Delta\Phi\right) = \tanh\left(l_s/\mu_s\right)\cdot\tan\left(l_s/\mu_s\right) \tag{18b}$$

where $I_F(I_R)$ is the absorbed light intensity for front (rear) illumination. PA saturation was assumed in deriving Eq. (18). The value of the thermal diffusivity *via* μ_s in the signal amplitude ratio measurement is obtained from the slope of the curve S_F/S_R *vs.* modulation frequency. In contrast, Eq. (18b) exhibits no explicit dependence on the absorbed power and surface conditions, so that a single modulation frequency measurement is sufficient to

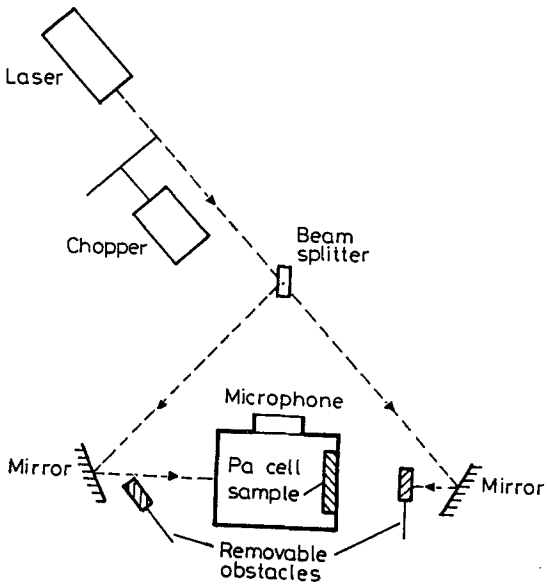

Fig 5 Schematic arrangement for the two-beam PA measurement of thermal diffusivity [from Ref. 38]

derive α_s. Extensive measurements of thermal diffusivities have been reported using the setup of Fig. 5, specifically on semiconductors [39] and insulators [40, 41].

Although the majority of thermal parameter determinations has been conducted photoacoustically using the gas-microphone cell, a certain amount of thermal studies has taken place using a piezoelectric crystal as transducer in Fig. 1. Lock-in detection of the PA signal is effected resulting from the acoustic waves launched in the solid due to thermal stress, and subsequently communicated to the transducer, which is an intimate contact with the sample. The piezoelectric PA theory developed by Jackson and Amer

[42] gives a theoretical expression for the voltage produced by the transducer, proportional to $\alpha(1+\nu)/\rho_s c_s$ when the thickness L of the transducer is smaller than l_s; α is the coefficient of linear expansion of the sample, ν is Poisson's ratio. However, when $L>l_s$, the signal is proportional to $\alpha E(1+\nu)/\rho_s c_s(1-\nu)$ for isotropic materials, where E is Young's modulus. Since $E(1+\nu)/(1-\nu) \propto B$ (bulk modulus), it follows that the PA signal in the case $L>l_s$ is proportional to the dimensionless Gruneisen parameter $\alpha B/\rho_s c_s$ of the sample. Exploiting this fact, Biswas *et al.* performed thermal characterization of coal and demonstrated the $\alpha B/\rho_s c_s$ dependence on 10 different coals of the Appalachian Basin.

d) FD photoacoustic thermal analysis in continuously inhomogeneous solids

PA depth profiling of inhomogeneous solids is a most important manifestation of the thermal analysis capabilities of this technique. Approximate formulations of the thermal-wave problem in solids with continuously varying thermal-thermodynamic parameters have been presented in the form of series expansions for thermal conductivity profiles and constant specific heat and sample density by Thakur [44]. However, the complexity of the final expressions for each profile and the lack of a criterion for the parameter ranges within which the infinite series expansions are well-behaved may be an obstacle in the direct use of these expressions with PA data. Perturbation-types of expansions for the thermal conductivity, $k_s(x)$, and specific heat, $c_s(x)$, about their surface values, $k_s(0)$ and $c_s(0)$, have been assumed for slightly inhomogeneous solids by Gusev *et al.* [45]. First-order regular perturbation theory was then used to obtain expressions for the thermal-wave field, but no attempt was made to invert the PA signal. A rigorous approach to the inverse thermal-wave problem has been presented by Vidberg *et al.* [46] These workers addressed the rather special situation of thermal-wave surface signals obtained by measuring the radial variation of the surface temperature of a continuously inhomogeneous solid about a heated point at a single modulation frequency. Both thermal conductivity and heat capacity profiles were reconstructed using Padé approximants for the inversion of spatial Laplace transforms, however, several constraints accompany the technique of Vidberg *et al.* The most important ones are the very specialized experimental geometry for which it is only valid and the fact that the theoretical problem is ill-posed and thus the reconstructed thermal profiles are not always numerically reliable. The same group [47] has also presented a numerical analysis of the same geometry based on the solution of the thermal-wave equation.

$$\nabla \cdot \left[k_s(\mathbf{r}) \nabla T(\mathbf{r}) \right] - i\omega \rho_s(\mathbf{r}) c_s(\mathbf{r}) = \frac{1}{2} \eta \beta I_0 \exp\left(-\beta \mid \mathbf{r} \mid \right) \quad (19)$$

with the temperature field

$$\theta(\mathbf{r}, t) = T(\mathbf{r}) e^{i\omega t}$$

based on a two-dimensional finite difference grid. Thermal-wave phase derived diffusivity profiles were thus obtained for surface hardened steel.

Very recently, Mandelis *et al.* [48] presented an application of the Hamilton–Jacobi formulation of thermal-wave physics [49] to the problem of PA depth profiling of general in homogeneous solids with arbitrary, continuously varying thermal diffusivity profiles, pertinent to the one-dimensional version of Eq. (20). A working general method for solving the inverse problem and obtaining arbitrary diffusivity depth profiles was demonstrated with excellent profile reconstruction fidelity. The generalized solutions obtained as a function of frequency[48] were further applied to an observed change in the PA signal frequency response of the liquid crystal octylcyanobiphenyl (8CB) in the nematic phase at 37° upon the application of a transverse magnetic field [50]. Quantitative profiles of thermal diffusivity decreases extending to 20–30 μm below the liquid crystal surface were obtained, Fig. 6. These decreasing profiles are qualitatively consistent with earlier PA temperature scans of liquid crystals and are a measure of the extent of bulk reorientational effects due to the magnetic field, as well as the extent of the influence of the surface as a domain reorientation inhibitor in the kGauss

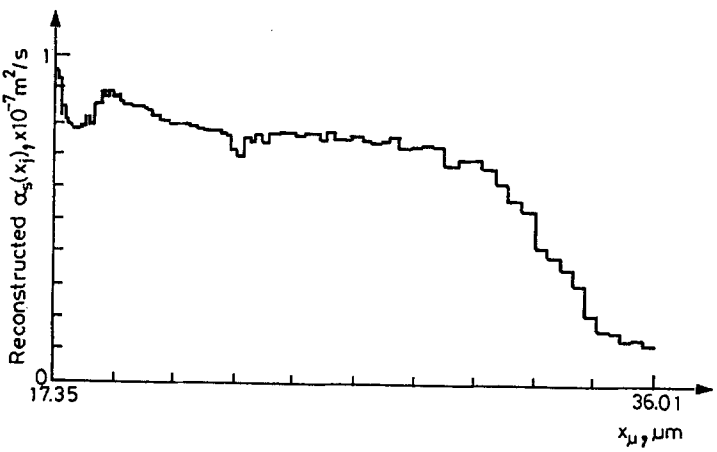

Fig 6 Reconstructed thermal diffusivity depth profile of a 8CB sample at 37.5° in the nematic phase with an applied transverse magnetic field B = 1.65 kG [from Ref. 50]

range. The main feature of this approach is its rich potential for PA thermal analysis of depth dependent thermo-physical phenomena.

e) T.D. photoacoustic detection

With the time-domain detection mode, a pulsed light source is used with no further modulation method. The signal processor, Fig. 1 is triggered by the source electronics to accept, store and display transient PA signal data. The TD detection method has not proven to be popular for either spectroscopic or thermal analysis purposes. A primary reason for this is the low frequency roll-off of the microphone transfer function [51], which limits the ability of cell-microphone based PA systems to yield accurate measurements of thermal transit times [52], on which transient thermal analysis relies. For the purposes of this review, other transient photothermal methods much more suitable for thermal analysis of solids will be presented. Such methods have definite advantages over PA detection, such as speed of response and ease of experimental implementation.

II. Photothermal methodologies

a) Photothermal beam deflection (Mirage effect) detection

In addition to PA techniques, several methods based on the deflection of a probe laser beam by a heated surface (PBD detection) have been implemented.[53–56] In this method a low-power laser beam (e.g. 1–2 mW He–Ne laser) skims the sample surface which is irradiated by an intensity-modulated optical beam. The thermal-wave generated by the light absorption in the solid and conducted to be surrounding (coupling) fluid (gas or liquid) induces a synchronous variation in the refractive index of the fluid due to the temperature dependence of the latter:

$$\Delta n_f(\omega) = \left(\frac{\partial n}{\partial T_f}\Big|_{T_f = T_o}\right) \Delta T_f(\omega) \tag{21}$$

As a result, a probe laser beam propagating near and parallel to the sample surface undergoes a deflection, generally away from the surface toward the region where n is higher ('Mirage effect'). In this case the transducer in Fig. 1 is a position sensitive semiconductor detector, which monitors the amplitude and phase of the detection and feeds the

preamplified PBD signal to the signal processor (lock-in amplifier). Figure 7 shows the basic concept and the three-dimensionality nature of the PBD method [57]. Due to the inherent three-dimensionality of laser pump beam sources, extraction of thermal parameters *via* this technique is generally more involved than PA detection. Salazar *et al.* [58] have made a detailed study of the three-dimensional aspects of the application of PBD technique to the measurement of thermal diffusivities in solids. Several special cases of thermal diffusivity ranges were identified as "measurable" from the slope of the deflection *vs.* $f^{-1/2}$ plot, depending on the relative values of the thermal diffusion lenghts and sample thickness in the photothermal saturation limit. Detailed measurements based on very similar theoretical considerations were made by Kuo *et al.* [59] and a list of the obtained thermal diffusivities from wide classes of materials is shown in Table 4. These values were obtained using the frequency dependence of the separation parameter x_o between the $+90°$ and $-90°$ phase points relative to the probe beam position at $x = 0$. The phase of the lock-in was set so that these 90° phase points correspond to zero crossings of the in-phase, Φ_t, signal (see Fig. 7. Furthermore, the assumption was made that

$$x_o = (\pi \alpha_s / f)^{1/2} + d \tag{22}$$

where d is a constant related to the (pump) heating beam diameter. x_o was then plotted *vs.* $f^{-1/2}$ and the slopes of the straight-line plots determined the values in Table 4. The use of Eq. (22) was further backed by three-dimensional calculations of the thermal-wave temperature field produced by Gaussian laser beams and integration over the probe beam profile [60]. The same group has also presented the application of the PBD technique as described above to the measurement of the diffusivity of a partially coated platform of a nickel-based alloy turbine blade [61], showing the feasibility of characterizing the thermal properties of coated materials. Thermal analysis of thin solid films has been carried out by Skumanich *et al* [62] using PBD detection in the limit where the pump beam width is significantly greater than the film thickness, so that heat conduction would be one-dimensional. These authors switched the probe beam from front to back of the sample and measured the PBD signal amplitude ratio:

$$\ln \left| T(l_s)/T(0) \right| = \ln 2 - (\omega/2\alpha_s)^{1/2} l_s \tag{23a}$$

and phase difference:

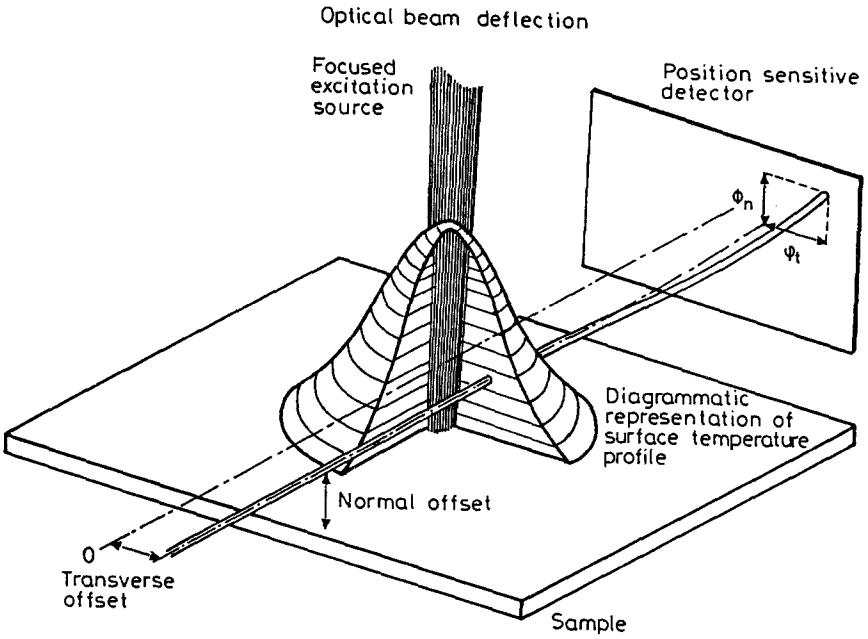

Fig 7 Schematic diagram of the PBD technique showing the passage if the probe beam through the thermal lens and resulting normal and transverse componenets of the PBD signal at the position sensitive detector [from Ref. 57]

$$\Delta\Phi = -(\omega/2\alpha_s)^{1/2} l_s \tag{23b}$$

In this manner, the diffusivities of Fe (200 μm), Cu (150 μm), Al (150 μm), Ge (45 μm) and amorphous hydrogenated Si (a–Si: H; 5 μm) were easily measured from the signal frequency dependence, without recourse to involved operations, due to the monodimensionality of the problem. An alternative configuration consists of a fixed probe beam skimming the surface, with the pump beam focused with a cylindrical lens into a narrow line of illumination on the film, parallel to the probe beam [62]. The pump beam is then displaced laterally along the film (y-direction) and the PBD signal is monitored as a function of lateral displacement y_o:

$$\ln\left|\text{ magnitude }\right| = \ln 2 - \left(y_o \cdot \sqrt{\pi/\alpha_s}\right) f^{1/2}, \tag{24a}$$

$$\text{phase} = -\left(y_o \cdot \sqrt{\pi/\alpha_s}\right) f^{1/2} \tag{24b}$$

The advantage of this technique is that no knowledge of the thin film thickness is required for calculating α_s. Of course, the major improvement over the aforementionad PBD embodiments is the judicious reduction of the 3–D problem to a 1–D experimental implementation with substantial simplifications in signal interpretation. This reduction, first introduced theoretically by Mandelis [56] has also been experimentally implemented in the thermal analysis of solids by Mandelis *et al.* [63–65]. These authors used frequency-multiplexed, time-delay domain PBD instrumentation, excitation and detection to study the thermal diffusivity of thin quartz samples supported by a black-painted backing. The nature of chirped modulation of the laser beam intensity, coupled with cross-correlation and spectral photothermal analysis [66], is such that it produces the transient impulse response of the sample.. The experimental implementation of time-delay domain PBD detection requires the replacement of the Signal Processor unit in Fig. 1 with a fast Fourier transform (FFT) dual channel Analyzer (e.g. HP 3562A) and connection of the chirped $X(t)$ output of this instrument to an A0 modulator, which provides the input waveform to the sample. The Nd: YAG beam used in the PBD experiments is transparent to quartz, but is efficiently absorbed by the black backing. The thermal-waveform thus generated traverses the sample thickness and difuses into the coupling fluid, where the probe laser beam skims the surface, an offset distance x_0 away. The Mirage effect thus causes a signal waveform $Y(t)$, which when properly amplified is cross-correlated with $X(t)$ in the FFT analyzer. It can be shown that

$$\tau_p(l_s) \approx \left[1 + 2(\alpha_f/\alpha_s)^{1/2}(l_s/x_0)\right](x_0^2/6\alpha_f) \tag{25}$$

where τ_p is the peak delay time of the impulse response and α_f is the coupling fluid thermal diffusivity. Equation (25) is valid for defocused jump beams, which guarantee 1–D behavior, and in the limit $(\alpha_f/\alpha_s)^{1/2} l_s << x_0$; otherwise, a quadratic term must be added. From the fit of experimental peak delay times to the data for various quartz thicknesses a straight line was obtained, in agreement with Eq. (25). Using the slope of the curve and Eq. (25) the diffusivity of quartz was found to be $4 \cdot 10^{-3}$ cm^2/s, in good agreement with literature values. The impulse response method has definite advantages over FD techniques with respect to thermal analysis of solids: the ease of interpretation of time-delayed peak responses, τ_p, in terms of sample thermal diffusivity *via* a single time-averaged transient signal measurement and FFT analysis provided in real time by the analyzer, compared

Table 4 Experimental values of thermal diffusivities measured from PBD signal *vs.* $f^{-1/2}$ plots [from Ref. 59]

Material	Thermal diffusivity, cm^2/s	
	This work	Nominal
	(WSU)	
Al	0.98	0.98
Au	1.29	1.28
Cr	0.31	0.29
Cu	1.31	1.16
Gd	0.059	0.057
Pb	0.28	0.24
Pt	0.31	0.25
Zn	0.45	0.42
Al alloy (2024)	0.54	
Armco iron	0.25	
Si3N4	0.23	
SiC	0.31, 0.66*	
	(ESPCI/EM^2)	
GaAs	0.26	0.21–0.26
Si	0.85	0.88
GaSb	0.27	0.24
InAs	0.19	0.19
InP	0.66	0.46

* Two differently prepared speciments

to a time-consuming series of many time-averaged frequency measurements, followed by external data reduction procedures.

b) Photothermal radiometric (PTR) detection

A popular photothermal technique well suited for non-contact thermal analysis of solids is based on the increase in black-body radiation emitted by an optically excited sample, the temperature of which increases as the result

of the optical energy absorption and subsequent nonradiative de-excitation and thermalization. A suitable infrared (IR) detector is used as the transducer in Fig. 1 and the (usually transient) signal is recorded. Pulsed laser photothermal radiometry (PPTR) has been developed for the study of thermal diffusivity of opaque (i.e. photothermally saturated) materials, within a few microns from the surface [67, 68]. Figure 8 shows the experimental setup for PPTR detection (front and rear-surface). The theory of PPTR was presented by Leung and Tam [70, 71]. For a semi-infinite homogeneous sample of absorption coefficient β and thermal diffusivity α_s, the transient back-scattered thermal emission signal from the surface is given by:

$$S(t) = C \exp(t/\tau\beta)\, erfc\left[(t/\tau\beta)^{1/2}\right] \tag{26}$$

where $\tau\beta$ is defined in Eq. (2), and C is a time-independent constant. Tam and Sullivan [67] showed that the thermal diffusivity of a transparent coating on black rubber backing can be obtained from

$$\tau_p = l_c/2\,\alpha_c \tag{27}$$

where τ_p is the peak delay time for the PPTR signal. They used a $l_c \approx 40\,\mu$m-thick transparent polyester coating, with $\alpha_s \approx 1 \cdot 10^{-3}$ cm^2/s, and measured $\tau_p \approx 8 \cdot 10^{-3}$ s. The technique also proved capable of sensing the mean thermal properties of powered black carbon-loaded epoxy samples, which were found to have a strong dependence on the degree of agglomeration. Imhof *et al.* [72] thus performed thermal analysis of hard and soft anodized aluminium oxide samples of complex structure, exhibiting pitting and deep pores. The long-time representation of the solution to the back-scattered transient photothermal problem leading to Eq. (26) which is valid at early times, $t \lesssim \tau\beta$, was shown to involve an exponential decay, $\exp(-t/\tau)$ with the time constant

$$\tau = l^2/s\,\alpha_s \tag{28}$$

where l, α_s are the thickness and diffusivity of the surface film, respectively, and s is an empirical 'substrate' constant. Decay profile dependence on β_s disappears at long times after the excitation, as the time-domain photothermal saturation condition (2) holds [11]. PPTR has found in recent years applications to the thermal analysis of composite [73, 74] and multilayered

materials [75]. Thermal localization and characterization of delaminating in a carbon-epoxy laminate was demonstrated [73] and depths of defects were measured. Table 5 shows *in-vivo* thermal analysis of the human skin [74] using a four-layer model [76]. Cielo *et al.* [77] presented a modified PPTR thermal-wave technique for the thermal analysis of bulk and thin-sheet materials. An annular-shaped area is heated by a pulsed laser beam focused on the material surface and the surface temperature is monitored by an IR detector focused at the center of the annulus. The converging action of the thermal flux results in a high magnitude of the detected signal with little

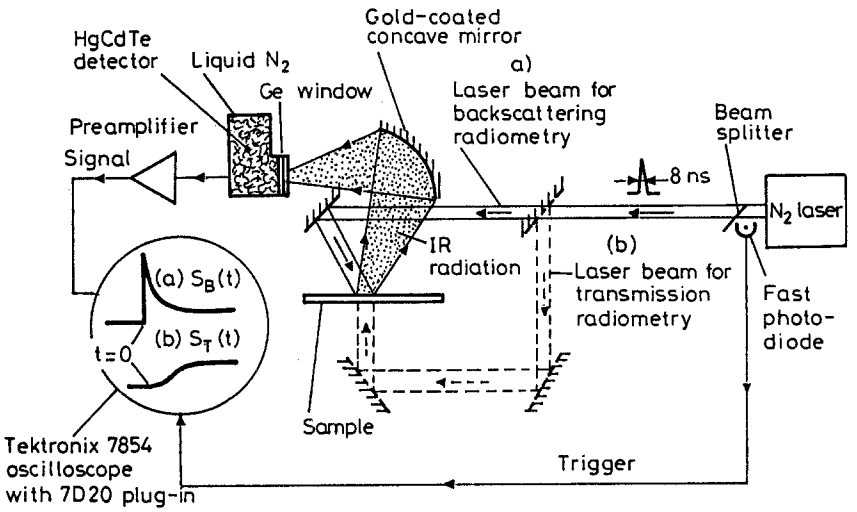

Fig. 8 Experimental setup for both single-ended back-scattering (laser beam represented by solid lines) and double ended (laser beam represented by dashed lines) PPTR measurements [from Ref. 69]

Table 5 Thermal properties of living human skin [from Ref. 74]

Nature of layer	Thickness, mm	Conductivity, $W\,m^{-1}\,K^{-1}$	Density, $10^3\,kg\,m^{-3}$	Spesific heat, $kJ\,kg^{-1}\,K^{-1}$	Diffusivity, $10^{-8}\,m^2\,s^{-1}$	Effusivity, $kJ\,m^{-2}\,s^{-1/2}\,K^{-1}$
Horny layer	0.1	0.21	3.6	1.2	4.9	0.95
Basel layer	0.1	0.42	3.6	1.2	9.7	1.34
Subcutaneous Vascular layer	0.6	0.42	3.6	1.2	9.7	1/34
Deep fat layer	some mm	0.17	2.3	0.92	7.9	0.60

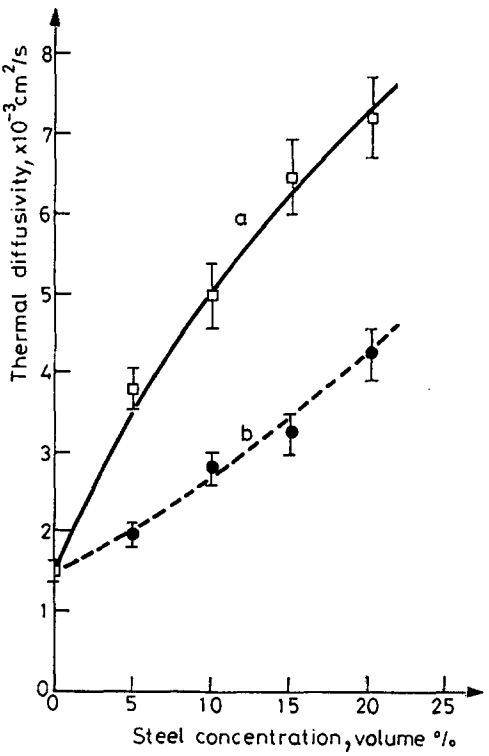

Fig. 9 Experimental results for the thermal diffusivity of a steel- polypropylene composite sheet as a function of steel concentrations. Curve (a) shows the values parallel to the surface measured by the convergent-wave technique; Curve (b) shows the values parallel to the surface as measured by the laser-flash technique [69] [From Ref. 77]

overheating of the irradiated material. Figure 9 shows typical thermal diffusivity results of the technique. Its high potential for implementation in an industrial remote inspection environment and quantitative thermographic analysis is bound to advance the development of this technique and of the entire field of PPTR, in general, in the area of thermal analysis.

c) Photopyroelectric (PPE) detection

Among the photothermal detection schemes, a recently developed pyroelectric technique [78, 79] is based on the detection of photothermal waves (modulated or transient) at the back-surface of a sample in intimate contact with a thin-film polyvinylidene fluoride (PVDF) pyroelectric polymer. The advantages of the PPE technique over other photothermal methods are extreme sensitivity (10 pJ) with very high time resolution

(~100 ps) at low cost ($ 0.10 /detector). The theory of the photopyroelectric effect has been developed [80] and has been shown to render this detection method very suitable for the thermal analysis of condensed phases in the photothermal saturation regime. Yeack *et al.* [81] used a PZT pyroelecric detector and pulsed CO_2 laser excitation to measure the diffusivity α_s of thin Mylar films, surface-coated with an opaque nichrome film to assure a surface heat source configuration. The fit of a one-dimensional transient heat conduction theoretical expression in the Equation [81]

$$V(t) = e^{-t/\tau_e} \int_0^t dt' e^{t'/\tau_e} \cdot \frac{pA}{C_A + C_P} \cdot \frac{d}{dt'} \overline{\theta_P(t')} \tag{29}$$

to the data was good, especially in the neighborhood of the transient peak, the temporal position of which is sensitive to the value of α_s, which is thus measured accurately. In Eq. (29), $V(t)$ is the pyroelectric voltage; τ_E is the electronic time constant of the element–preamplifier system; p is the element pyroelectric coefficient; C_A and C_P are the detector and preamplifier capacitances, respectively; and $\overline{\theta_P(t)}$ is the spatial average, with respect to the pyroelectric element thickness, of the temperature in the transducer. More recently Power and Mandelis [82] used chirp time-delay domain spectrometry (FM–TDS) to obtain the photopyroelectric impulse response from several materials (fused quartz, stainless steel and aluminium) as detected by a thin PVDF film sensor in back-side contact with the sample. The thin-film response was shown to be more sensitive to thermal conductivity values than that from a thick pyroelectruc [83]. Figure 10 shows the excellent fit of the theory to the experimental impulse response from quartz. A comparison between the fit at early times of Figure 10 with that by Yeack *et al.* [81] gives unequivocal evidence of the advantages of using FM–TDS over single-pulse excitation in cases where pulse length and response observation times may overlap, even partially. In order to obtain the photothermal impulse response to a laser pulse from a thin- film resin sample (NOVOLAC™ film), free from artifacts due to the PVDF pyroelectric transducer impulse response itself in the sub-ms time domain, Coufal and Hefferle used a quasi-theoretical/quasi-numerical data fitting procedure [84]. This type of procedure is necessary with thin films, when both detector and sample impulse response temporal domains heavily overlap. It is quite powerful and simple as it accounts for the actual response of experimental pyroelectric circuits without complicating circuit modelling factors, however, it may be altogether avoided with non-thin-film specimens. In such cases, appropriate

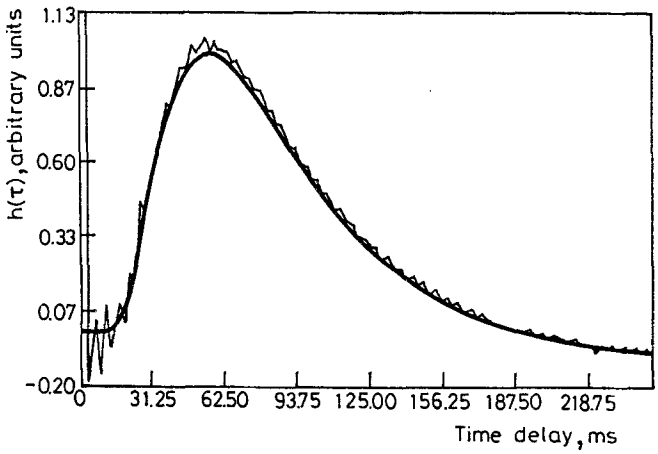

Fig. 10 Time-delay-domain (TDS) PVDF photopyroelectric impulse response from a 500 μm, quartz sample surface-coated with an opaque thin film. Best fitting parameters to one-dimensional heat conductionmodel:[83] $\alpha_{Quartz} = 4.4 \cdot 10^{-7}$ m^2/s; $k_{Quartz} = 2.2$ W/m K [From Ref. 82]

frequency-multiplexed detection techniques and a judicious choice of the exciting frequency bandwidth may be used so that the input signal autocorrelation function and the bare detector input-output cross-correlation function will be delta-function-like in the time scale of the maximum sample response [66].

A different a very simple method for obtaining accurate values for the thermal diffusivity of materials involves using frequency-domain techniques (either chopped excitation and point-by-point lock-in detection or frequency-sweep excitation and FFT detection) to obtain the laser-induced photopyroelectric transfer function of the sample/detector system. A discontinuity in the amplitude frequency response has been predicted for photothermal detection [85], when the thermal diffusion lenght in the sample becomes equal to its thickness (i.e. the sample is in the transition region between thermally thick and thermally thin). This effect has been demonstrated under photopyroelectric detection as well [79] for a single layer solid; and for a double layer system involving several types of samples (metal, semiconductor and thermal insulator ranging in thickness between 60 μm and 500 μm, and covering several orders of magnitude in thermal diffusivity) supported by a layer of thermally conducting grease [85] on PVDF. Thin-film NOVOLAC™ samples, coated on PVDF, 0.65–2.45 μm thick were successfully analyzed and the diffusivity extracted from the slopes of the transfer functions and from the relative photothermal phase shifts, in a fre-

quency-domain experiment parallel to the pulsed time-domain technique described earlier [84]. Similar photopyroelectric thermal diffusivity measurements in the frequency-domain were recently reported [86] for five polymeric materials (PVDF, PVF, low-density polyethylene, polypropylene, Teflon, as well as a commercial PZT and a tin-substituted PZT). The thicknesses ranged between several micrometers and one millimeter. The thermal diffusivity was estimated by matching the experimental phases to a one-dimensional analytical solution to the heat conduction equation using a minimization algorithm. The resolution and accuracy of the frequency domain photopyroelectric determination of thermal diffusivity of a thin sample are trade-offs between large enough sample thickness and low enough diffusivity to induce a measurable change in slope of the amplitude response or a detectable shift in the phase. A substantial increase in resolution may be effected by modifying the conventional one-dimensional detection geometry [87], so that a portion of the lateral dimensions of the sample behaves in a thickness-like manner. Scanning this lateral dimension at fixed modulation frequency has an effect similar to scanning modulation frequencies in the photopyroelectric response, and thermal diffusivity may be readily calculated.

III. Non-conventional photothermal applications to thermal analysis

a) Phase transitions

Photothermal techniques are very well suited for monitoring such transitions in the thermal/thermodynamic parameters of solids. Theoretical and experimental activity has occurred at both high temperature and low temperature thermal behavior of materials. Bechthold *et al.* [88] studied phase transitions in metal hydrogen interstital alloys (Nb–, Ta–, and V–hydrides) by means of temperature-dependent PA detection in the 300–500 K range. First and second order phase transitions were observed and the results from thermally thick samples in the PA saturation regime were found to be in agreement with a PA model [89] including the latent heat involved in the phase transition and assuming two different thermal states present in the sample during the phase transition. These authors farther showed that the PA method can be used to study phase diagrams. Both amplitude and phase of the specially built high-temperature cell exhibited sharp variations at the phase transition temperature, reflecting the behavior of the thermal effusivity, Fig. 11. PA detection was also used [90] for the study of the glass

transition region of the supercooled salt melt 0.4 $Ca(NO_3)_2$ – 0.6 KNO_3. The transition temperature was determined by the maximum in the phase angle. A frequency-dependent specific heat was calculated in the dispersion region as the quantity in the effusivity e_s, Eq. (9), mostly sensible for the transition. Semiconducting materials undergoing phase transitions, such as the para-ferroelectric transition in SbSI crystals have been studied [91]. In this case it is the optical absorption coefficient which is responsible for the transition at 300 K and ~3.41 eV; PA detection was found suitable due to its sensitivity to the value of β_s in the non-saturated regime. Low-temperature PA phase tran-

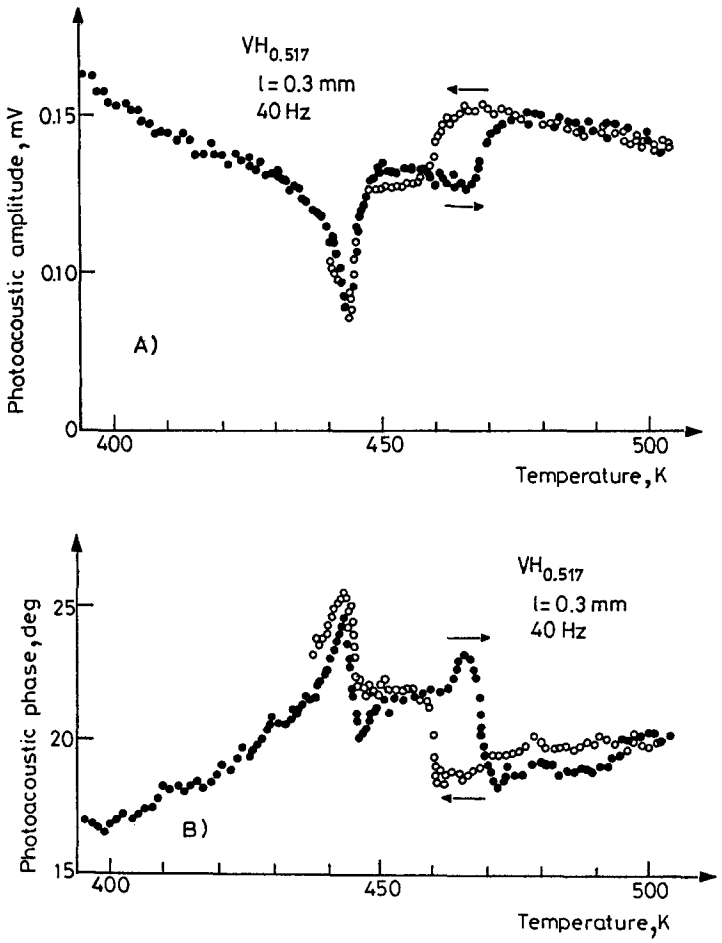

Fig. 11 Phase transitions in $VH_{0.517}$ as monitored by PA amplitude (A) and phase (B) temperature scans. $\beta \rightarrow \varepsilon$ and $\varepsilon \rightarrow \alpha$ transitions are observed at 445 and 466 K, respectively. Hysteresis in the (first order) $\varepsilon \rightarrow \alpha$ transition is also observed [from Ref. 88]

sition studies usually require complicated instrumentation due to the inability of microphones to operate cryogenically [92, 93]. Under these conditions non-saturated samples exhibit a PA response [7] $\propto c_s\ (T^{-1})$, whereas optically opaque, saturated samples behave [7] $\propto [c_s(T)k_s(T^{-1/2})$. In the former category Pichon *et al.* [92] studied the specific heat anomaly of the insulators $CrCl_3$ and MnF_2 in the neighborhood of structural (magnetic) phase transitions ($\sim$ 15 K and 65 K, respectively). In the latter category, Siqueira *et al.* [93] derived experimental plots of the *product* $c_s(T)k_s(T)$ of Al-doped VO_2 around the structural phase transition at 320 K. Phototpyroelectric detection of the same transition was shown to be superior [94] on two grounds: first, the extreme simplicity of the technique, which does not require special heating or cooling shielding, second, its rear-surface detection character results in direct PPE signal dependence on $c_s(T)^{-1}$ only for opaque solids [80]. VO_2 phase transitions have also been studied using frequency domain PTR. With this detection technique, the *product* $c_s(T)k_s(T)$ is monitored [95] similar to a PA detection, however, there is the additional advantage of remote, non-contact detection.

Very popular phase transitions for photothermal detection have been melting transitions. Latent heats of melting are responsible for discontinuities in the FD or TD signals. Florian *et al.* [96] studied Ga melting, and so did Kojima [97] who produced images of the spatial variation of PA amplitude in the vicinity of the liquid-solid transition temperature [98]. Imhof *et al.* [99] used PPTR to monitor the melting transition of benzophenone at 48°. This technique demonstrated the potential for studying re-crystallization dynamics during pulsed laser annealing and other surface treatments. In addition, relative thermal diffusivities in the solid and liquid phases, and a measure of the initial surface temperature jump caused by the absorption of the laser pulse were obtained.

Another important facet of photothermal investigation and thermal analysis of solid state transitions is the increasing recent use of these techniques in the study of superconducting transitions. PA measurements have provided information on either the diffusivity [100] or the effusivity [101] in the superconducting transition region of high-T_c superconductors. At this time it appears that the PPE technique has an advantage over the PA method, in that it is capable of the *simultaneous* determination of specific heat, thermal conductivity and thermal diffusivity and can thus be used to obtain the T-dependence of these parameters, including the superconducting transition region. FD measurements have been performed by Marinelli *et al.* [102], whereas time-delay domain impulse response measurements have been reported by Peralta *et al.* [103] Table 6 shows thermal analysis results

from the impulse response data. The advantage of this method over the FD detection [102] is that it does not require a calibration procedure for the

Table 6 Summary of measurements for thermal parameters of $YBa_2Cu_3O_{7-x}$ from the literature and as measured by FM–Time Delay Photopyroelectric Spectrometry [from Ref. 103a]

$\alpha(T_c)$, cm^2/s	α(300 K), cm^2/s	$\kappa(T_c)$, W/m·K	κ(300 K), W/m·K	$\Delta C/C$	Ref.
–	–	5.00	5.00	–	[a]
–	–	3.50	4.75	–	[b]
0.0130	0.0070	–	–	0.050	[c]
0.0230	0.0100	–	–	0.060	[d]
0.0225	0.0120	–	–	0.060	[d]
0.0375	–	2.75	–	–	[e]
0.0525	–	5.40	–	0.025	[f]
–	0.0710	–	–	–	[g]
–	0.0458	–	–	–	[g]
–	–	3.00	2.20	–	[h]
0.0140	0.0090	4.00	4.75	0.040	This work

[a] D. T. Morelli, J. Heremans, D. E. Swets: Phys. Rev. B36, 3917 (1987)

[b] C. Uher, A. B. Kaiser: Phys. Rev. B 36, 3917 (1987)

[c] Ref.100

[d] Ref. 103b

[e] F. Murtas, M. G. Mecozzi, M. Marinelli, U. Zammit, R. Pizzoferato, F. Scudieri, S. Martellucci, M. Marinelli: In *Photoacoustic and Photothermal Phenomena II*, ed. by J. C. Murphy, J. W. Maclachlan Spicer, L. C. Aamodt, B. S. H. Royce, Springer Ser. Opt. Sci. Vol. 62 (Springer, Berlin, Heidelberg 1990) pp. 208–210

[f] Ref. 102

[g] X. Zhang, C. Gan, Z. Xu, S. Zhang, H. Zhang: In *Photoacoustic and Photothermal Phenomena II*, ed. by J. C. Murphy, J. W. Maclachlan Spicer, L. C. Aamodt, B. S. H. Royce, Springer Ser. Opt. Sci. Vol. 62 (Springer, Berlin, Heidelberg 1990) pp. 205–207

[h] V. Bayot, F. Delannay, C. Dewitte, J.–P. Erauw, X. Gonze, J.–P. Issi, A. Jonas, M. Kinany–Alaoui, M. Lambricht, J.–P. Michenaud, J.–P. Minet, L. Piraux: Solid State Commun. 63, 983 (1987)

[j] M. Muller, R. Osiander, A. Gold, P. Korpiun: In *Photoacoustic and Photothermal Phenomena II*, ed. by J. C. Murphy, J. W. Maclachlan Spicer, L. C. Aamodt, B. S. H. Royce, Springer Ser. Opt. Sci. Vol. 62 (Springer, Berlin, Heidelberg 1990) pp. 198–201

pyroelectric transducer. Overall, PPE detection appears to be optimal among photothermal methods for superconducting transition studies due to its very broad temperature range response ability especially at cryogenic temperatures and the ability for simultaneous measurement of several thermal functions.

b) Broader thermal analysis

Photothermal-based techniques have been increasingly applied to other areas of thermal analysis. In this section a selection of promising new areas will be presented. The new applications of laser pulse-induced desorption of thin layers from surfaces [104] is an intriguing mixture of photochemical and photothermal phenomena. Single shot time-of-flight molecular distributions measured following ultraviolet laser pulse excitation of surfaces have been found to obey modified Maxwellian velocity distributions upon conversions of surface thermal (absorbed) energy into molecular kinetic energy [105, 106]. Photothermal desorption and ablation was reported for the system NO on Ag (111) [107]. Several advances in the spectroscopy of surfaces and adsorbates have been made using pyroelectric detection. Polarization modulation spectroscopy is based on the selective absorption of either *s*– or *p*–polarized light waves, phase shifted by 180°. The technique has been applied as a real-time compensation scheme by adjusting the relative amplitude of the electric field vector for the two polarizations, in such a way as to obtain a zero substrate signal from an Ag film evaporated *in situ* directly on a pyroelecrtic ceramic sensor [108]. Then NH_3 molucules were slowly allowed to adsorb on Ag under UHV conditions, giving rise to a photothermal signal due to the selective absorption of the *p*-polarized light of a cw CO_2 laser tuned to 9.3 μm (1075 cm^{-1}) to excite the ν_2 vibrational transition of NH_3. This detection method permits recording photothermal signals induced by an *unstabilized* cw laser with a sensitivity of fractions of a monolayer (e.g. $5 \cdot 10^{-3}$) of a monolayer for the NH_3–Ag system, Fig. 12). Furthermore, without employing compensation or signal averaging techniques, a sensitivity corresponding to a surface coverage of $2 \cdot 10^{-3}$ of a monolayer for the SF_6 on silver was achieved under UHV conditions. [109] Under similar conditions, time-dependent phenomena like the adsorption/desorption cycle on SF_6 on silver [110] and the adsorption of NH_3 on silver [111] were readily observed [111]. Coufal [78] carried out surface spectroscopic pyroelectric studies of a Nd_2O_3 sample containing $8 \cdot 10^{14}$ molecules isolated in a 10 μm thick poly (methyl methacrylate) matrix, corresponding approximately to a one-monolayer coverage of Nd^{3+} ions, using a

PVDF detector. Photothermal spectra were thus obtained under both harmonically modulated and pulsed dye laser excitation in the 400–700 nm

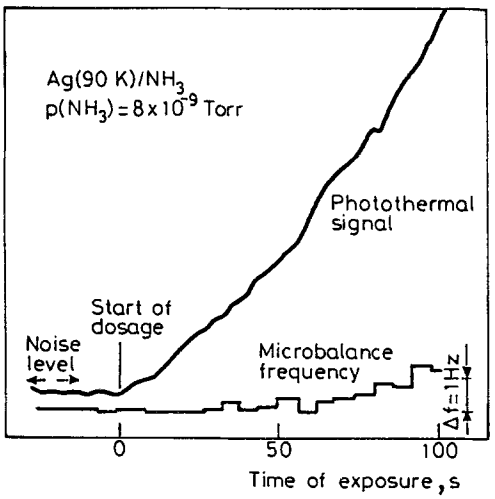

Fig. 12 Polarization-modulated photopyroelectric signal and microbalance readout as a function of time as ammonia molecules are slowly adsorbed on the silver substrate. The maximum coverage is $\theta = 0.80$. The noise level is indicated on the left hand side for the clean substrate. Shortly before the dosage is started, the noise increases slightly while the dosage valve is opened. The ammonia partial pressure in the system is $8 \cdot 10^{-9}$ Torr. [from Ref. 108]

region, demonstrating the strong spectroscopic potential of the photopyroelectric technique for surface species characterization at a sensitivity of hundredths of a monolayer. Pyroelectric *in-situ* detection of the reduction of a film CuO surface oxide layer into metallic Cu by diluted HCl has further demonstrated the ability of the method to monitor interfacial chemistry and measure rate constants [79].

A promising new approach involves the combined use of PA spectroscopy and differential thermal analysis in applications such as the identification of minerals and of processes that take place during their alteration [112]. The ultraviolet-infrared PA spectra of a series of minerals (iron oxides and oxyhydroxides, carbonates, silicates, bauxite and gypsum) were studied for changes due to heating and a better identification of chemical species in these minerals was possible that with differential thermal analysis (DTA) and thermogravimetry (TG) alone. Of course, a photothermal spectroscopy, such as PAS, is essential for the characterization of such raw materials, which are not easily handled by purely optical spectroscopies [2].

Conclusion

In this review the following directions appear to emerge for future applications of the rich arsenal of photothermal techniques to thermal analyses of solids: i) The abovementioned techniques do now, and will in the future, play an unequivocally leading role in the most convenient and accurate determination of thermal transport properties: thermal diffusivity, effusivity, conductivity and, indirectly, specific heat. ii) Detailed studies of the physics of phase transitions are emerging and will likely proliferate, due to the very high degree of background temperature controllability as well as of the thermal-wave probe exhibited by all photothermal techniques. iii) Combinations of photothermal with other complementary conventional thermal analysis methods may prove rewarding, due to the ease and simplicity of the implementation of photothermal experiments; as a result new knowledge about the thermal behavior of matter, not previously accessible, may now emerge, such as the *in-situ* measurement of interfacial thermodynamics, enthalpies of multiphase transitions etc. iv) It has become apparent that good opportunities exist in the multidisciplinary domain on non-intrusive, highly sensitivity and fast thermal analysis, a field still largely undeveloped, but with great potential due to the increasing availability of modern laser techniques, such as the emerging ultrafast photothermal detection [113]. Such development will no doubt help launch a new and exciting era in the evolving field of Thermal Analysis.

* * *

I wish to gratefully acknowledge the continuous support of the Ontario Laser and Lightwave Research Center (OLLRC) and of the Natural Sciences and Engineering Research Council of Canada (NSERC), for much of the research performed in my Laboratory as described and discussed in this Review.

References

1 Y. H. Pao, Optoacoustic Spectroscopy and Detection, Academic, New York 1977.
2 A. Rosencwaig, Photoacoustics and Photoacoustic Spectroscopy, Chemical Analysis, Vol. 57 Wiley, New York 1980.
3 A. Mandelis (ed.), Photoacoustic and Thermal Wave Phenomena in Semiconductors, North-Holland, New York 1987.
4 H. Coufal and A. Mandelis, Ferroelectrics (in press).
5 D. A. Hutchins and A. C. Tam, IEEE Trans. Ultrason., Ferroel., Freq.Control, UFFC-33, 429 (1986).

6 J.-P. Monchalin, IEEE Trans. Ultrason., Ferroel., Freq. Control, UFFC-33, 485 (1986).
7 A. Rosencwaig and A. Gersho, J. Appl. Phys., 47 (1976) 64.
8 W. B. Jackson, N. M. Amer, A. C. Boccara and D. Fournier, Appl. Opt., 20 (1981) 1333.
9 R. Santos and L. C. M. Miranda, J. Appl. Phys., 52 (1981) 4149.
10 A. Mandelis and M. M. Zver, J. Appl. Phys., 57 (1985) 4421.
11 A. Mandelis and B. S. H. Royce, J. Appl. Phys., 50 (1979) 4330.
12 J. G. Parker, Appl. Opt., 12 (1873) 2974.
13 M. J. Adams and G. F. Kirkbright, Spectrosc. Lett., 9 (1976) 255.
14 L. R. Ingersoll, O. J. Zobel and A. C. Ingersoll, Heat Conduction, Univ. Wisconsin Press, 1954.
15 V. E. Lyamov, U. Madaliev and R. E. Shikhlinskaya, Teplofiz. Vysok. Temp., 19 (1981) 93. [English Trans.]
16 A. Lachaine and P. Poulet, Appl. Phys. Lett., 45 (1984) 953.
17 K. N. Madhusoodanan, M. R. Thomas and P. Jacob, J. Appl. Phys., 62 (1987) 1162.
18 B. K. Bein, H. W. Schmidt, J. Gibkes, J. Pelzl and P. S. Bechthold, Proc. 6th Int. Top. Meet. on Photoacoustic and Photothermal Phenomena II, J. C. Murphy, J. W. Maclachlan Spicer, L. C. Aamodt and B. S. H. Royce, Eds. Springer-Verlag, Berlin 1990 p. 86.
19 B. K. Bein and J. Pelzl, Proc. 4th Int. Carbon Conf. CARBON 86, Baden-Baden, Deutsche Keram. Gesellschaft, 1986, p.268.
20 B. K. Bein, S. Krüger and J. Pelzl, Proc. 4th int Carbon Conf. CARBON 86, Baden-Baden, Deutsche Keram. Gesellschaft, 1986, p. 231; B. K. Bein, S. Krueger and J. Pelzl, J. Nucl. Mat., 119 (1986) 141; B. K. Bein, S. Krueger and J. Pelzl, J. Nucl. Mat., 145 (1987) 458.
21 A. Mandelis, Y. C. Teng and B. S. H. Royce, J. Appl. Phys., 50 (1979) 7138.
22 N. C. Fernelius, J. Appl. Phys., 51 (1980) 650.
23 T. Papa, F. Scudieri and D. Sette, Nuovo Cimento, 1D (1982) 129.
24 U. Zammit, M. Marinelli, F. Scudieri and S. Martelucci, Appl. Phys. Lett., 50 (1987) 830.
25 A. Mandelis and J. D. Lymer, Appl. Spectrosc., 39 (1985) 473.
26 H. W. Godbee and W. T. Ziegler, J. Appl. Phys., 37 (1966) 40; and J. Appl. Phys., 37 (1966) 56.
27 B. K. Bein, U. Bertsch, W. Rubelowski, M. M. F. d'Aguiar Neto nad J. Pelzl, Proc. 6th Int. Top. Meet. on Photoacoustic and Photothermal Phenomena II, J. C. Murphy, J. W. Maclachlan Spicer, L. C. Aamodt and B. S. H. Royce, Eds. Springer-Verlag, Berlin 1990 p.82.
28 S. Aithal, G. Rousset, L. Bertrand, P. Cielo and S. Dallaire, Thin Solid Films, 119 (1984) 153.
29 P. Charpentier, F. Lepoutre and L. Bertrand, J. Appl. Phys., 53 (1982) 608.
30 R. T. Swimm, Appl. Phys. Lett., 42 (1983) 955.
31 B. Bonno, J. L. Laporte and Y. Rousset, J. Appl. Phys., 67 (1990) 2253.
32 T. Hashimioto, J. Cao and A. Takaku, Thermochim. Acta, 120 (1987) 191.
33 P. Korpiun, B. Merté, G. Fritsch, R. Tilgner and E. Lüscher, Colloid & Polymer Sci., 261 (1983) 312.
34 H. G. Kilian and M. Pietralla, Polymer, 19 (1978) 664.
35 C. L. Choy and K. Young, Polyner, 18 (1977) 769.
36 L. F. Perondi and L.C. M. Miranda, J. Appl. Phys., 62 (1987) 2955.
37 G. Rousset, F. Lepoutre and L. Bertand, J. Appl. Phys., 54 (1983) 2383.
38 O. Pessoa, Jr., C. L. Cesar, N. A. Patel, H. Vargas, C. C. Ghizoni and L. C. M. Miranda, J. Appl. Phys., 59 (1986) 1316.
39 H. Vargas and L. C. M. Miranda, in Photoacoustic and Thermal Wave Phenomena in Semiconductors, A. Mandelis, Ed. North-Holland, New York 1987 Chap.6.
40 A. C. Bento, H. Vargas, M. M. F. Aguiar and L. C. M. Miranda, Phys. Chem. Glasses, 28 (1987) 127.
41 N. F. Leite, N. Cella, H. Vargas and L. C. M. Miranda, J. Appl. Phys., 61 (1987) 3025.
42 W. Jackson and N. M. Amer, J. Appl. Phys., 51 (1980) 3343.
43 A. Biswas, T. Ahmed, K. W. Johnson, K. L. Telschow, J. C. Crelling and J. M. Myers, Can. J. Phys., 64 (1986) 1184.
44 A. K. S. Thakur, Lett. Heat Mass Transfer, 9 (1982) 385.
45 V. Gusev, Ts. Veliniv and K. Bransalov, Semicond. Sci. Technol., 4 (1989) 20.
46 H. J. Vidberg, J. Jaarinen and D. O. Riska, Can. J. Phys., 64 (1986) 1178.

47 J. Jaarinen and M. Luukkala, J. Phys. (Paris), 44, C6 (1983) 503.
48 A. Mandelis, S. B. Peralta and J. Thoen, J. Appl. Phys., (in press)
49 A. Mandelis, J. Math. Phys., 26 (1985) 2676.
50 A. Mandelis, E. Schoubs, S. B. Peralta and J. Thoen, J. Appl. Phys., (in press)
51 A. Mandelis and B.S. H. Royce, J. Appl. Phys., 51 (1980) 610.
52 J. T. Dodgson, A. Mandelis and C. Andreetta, Can. J. Phys., 64 (1986) 1074.
53 A. C. Boccara, D. Fournier and J. Badoz, Appl. Phys. Lett., 36 (1980) 130.
54 J. C. Murphy and L. C. Aamodt, J. Appl. Phys., 51 (1980) 4580.
55 W. B. Jackson, N. M. Amer, A. C. Boccara and D. Fournier, Appl. Opt., 20 (1981) 1333.
56 A. Mandelis, J. Appl.Phys., 54 (1983) 3404.
57 L. C. Aamodt and J. C. Murphy, J. Appl. Phys., 52 (1983) 581.
58 A. Salazar, A. Sánchez–Lavega and J. Fernandez, J. Appl. Phys., 65 (1989) 4150.
59 P. K. Kuo, M. J. Lin, C. B. Reyes, L. D. Favro, R. L. Thomas, D. S. Kim, S. Y. Zhang, L. J. Inglehart, D./ Fournier, A. C. Boccara and N. Yacoubi, Can. J. Phys., 64 (1986) 1165.
60 P. K. Kuo, E. D. Sendler, L. D. Favro and R. L. Thomas, Can. J. Phys., 64 (1986) 1168.
61 R. L. Thomas, L. J. Inglefart, M. J. Lin, L. D. Favro and P. K. Kuo, Rev. Progr. Quant. Nondestr. Eval., D. O. Thompson and D. E. Chimenti, Eds. Plenum, New York Vol. 4B, 1985 p. 859.
62 A. Skumanich, H. Dersch, M. Fathallah and N. M. Amer, Appl. Phys., A43 (1987) 297.
63 A. Mandelis, Rev.Sci. Instrum., 57 (1986) 617.
64 A. Mandelis, L.M.-L. Borm and J. Tiessinga, Rev. Sci. Instrum., 57 (1986) 622.
65 A. Mandelis, L.M.-L. Borm and J. Tiessinga, Rev. Sci. Instrum., 57 (1986) 630.
66 A. Mandelis, IEEE TRans. Ultrason., Ferroel., Freq. Control, UFFC-33 (1986) 596.
67 A. C. Tam and B. Sullivan, Appl . Phys. Lett., 43 (1983) 333.
68 R. E. Imhof, D. J. S. Birch, F. R. Thornley, J. R. Gilchrist and T. A. Strivens, J. Phys. E: Sci. Instrum., 17 (1984) 521.
69 A. C. Tam, in Photoacoustic and Thermal Wave Phenomena in Semiconductors, A. Mandelis, Ed. North-Holland, New York 1987. Chap.8.
70 W. P. Leung and A. C. Tam, Opt. Lett., 9 (1984) 93.
71 W. P. Leung and A. C. Tam, J. Appl. Phys., 56 (1985) 153.
72 R. E. Imhof, F. R. Thornley, J. R. Gilchrist and D. J. S. Birch, J. Phys. D: Appl. Phys., 19 (1986) 1829.
73 D. L. Balageas, A. A. Deom and D. M. Boscher, Mat. Eval., 45 (1987) 2608.
74 D. L. Balageas, J. C. Krapez and P. Cielo, J. Appl. Phys., 59 (1986) 348.
75 L. C. Aamodt, J. W. Maclachlan Spicer and J. C. Murphy, J. Appl. Phys., 68 (1990) 6087.
76 J. A. Stolwijk and J. D. Hardy, J. Appl. Physiol., 20 (1965) 1006.
77 P. Cielo, L. A. Utracki and M. Lamontagne, Can. J. Phys., 64 (1986) 1172.
78 H. Coufal, Appl. Phys. Lett., 44 (1984) 59.
79 A, Mandelis, Chem. Phys. Lett., 108 (1984) 388.
80 A. Mandelis and M. M. Zver, J. Appl. Phys., 57 (1985) 4421.
81 C. E. Yeack, R. L. Melcher and S. S. Jha, J. Appl. Phys., 53 (1982) 3947.
82 J. F. Power and A. Mandelis, Rev. Sci. Instrum., 58 (1987) 2024.
83 J. F. Power and A. Mandelis, Rev. Sci. Instrum., 58 (1987) 2018.
84 H. Coufal and P. Hefferle, Appl. Phys., A38 (1985) 213.
85 P. K. John, L. C. M. Miranda and A. Rastogi, Phys. Rev. , B34 (1986) 4342.
86 S. B. Lang, Ferroelectrics, 93 (1987) 87.
87 C. C. Ghizoni and L. C. M. Miranda, Phys. Rev., B32 (1985) 8392.
88 P. S. Bechthold, M. Campagna and T. Schober, Solid state Commun., 36 (1980) 225.
89 P. Korpiun and R. Tilgner, J. Appl. Phys., 51 (1980) 6115.
90 B. Büchner and P. Korpiun, Appl. Phys., B43 (1987) 29.
91 M. Grandolfo, C. Ranghiasci, P. Vecchia and Sh. M. Efendiev, Ferroelectrics, 56 (1984) 87.
92 C. Pichon. M. Le Liboux, D. Fournier and A. C. Boccara, Appl. Phys. Lett., 35 (1979) 435.
93 M. A. A. Siquiera, C. C. Ghizoni, J. I. Vargas, E. A. Menezas, H. Vargas and L. C. M. Miranda, J. Appl. Phys., 51 (1980) 1403.
94 A. Mandelis, F. Care, K. K. Chan and L. C. M. Miranda, Appl. Phys., A38 (1985) 117.

95 S. Pekker and E. M. Eyring, Appl. Spectrosc., 40 (1986) 397.
96 R. Florian, J. Pelzl, M. Rosenberg, H. Vargas and R. Wernhardt, Phys. Stat Sol., A48 (1978) K35.
97 S. Kojima, Jpn. J. Appl. Phys., 24 (1985) 1571.
98 S. Kojima, Jpn. J. Appl. Phys., 25 (1986) 215.
99 R. E. Imhof, F. R. Thornley, J. R. Gilchrist and D. J. S. Birch, Appl. Phys., B43 (1987) 23.
100 L. Gomes, M. M. F. Vieira, S. L. Baldochi, N. B. Lima, M. A. Novac, N. D. Vieira, Jr., S. P. Morato. A. J. P. Braga, C. L. Cesar, A. F. S. Penna and J. Mendes Filho, J. Appl. Phys., 63 (1988) 5044.
101 Y. S. Song, H. K. Lee and N. S. Chang, J. Appl. Phys., 65 (1989) 2568.
102 M. Marinelli, F. Murtas, M. G. Mecozzi, U. Zammit, R. Pizzoferrato, F. Scudieri, S. Martellucci and M. Marinelli, Appl. Phys., A51 (1990) 387.
103 S. B. Peralta, Z. H. Chen and A. Mandelis, Appl. Phys. A (in press); S. B. Peralta, Z. H. Chen and A. Mandelis, Feroelectrics (in press)
104 P. Hess, in Photoacoustic, Photothermal and Photochemical Processes at Surface and in Thin Films, P. Hess, Ed. Springer-Verlag, Berlin 1989. Chap. 3.
105 M. Buck and P. Hess, J. Electron Spectrosc., 45 (1987) 237.
106 L. M Cousins and S. R. Leone, Chem. Phys. Lett., 155 (1989) 162.
107 W. C. Natzle, D. Padowitz and G. J. Sibener, J. Chem. Phys., 88 (1988) 7975.
108 H. Coufal, F. Träger, T. J. Chuang and A. C. Tam, Surf. Sci. Lett., 145 (1984) L504.
109 H. Coufal, T. J. Chuang and F. Träger, IBM Res. Report, RJ 4344 (1984).
110 F. Träger, H. Coufal and T. J. Chuang, Phys. Rev. Lett., 49 (1982) 1720.
111 T. J. Chuang, H. Coufal and F. Träger, J. Vac. Sci. Technol., A1 (1983) 1236.
112 M. C. Cresser and N. T. Livesey, Analyst, 109 (1984) 219.
113 A. Lörincz and A. Miklós, in Progresse in Photothermal and Photoacoustic Science and Technology, A. Mandelis, Ed. (North-Holland, New York in press).

Zusammenfassung — Es wird ein Rückblick auf die wichtigsten Anwendungen von optisch-induzierten Wärmewellen bei der thermischen und thermodynamischen Analyse von Feststoffen gegeben. Es wird das gesamte Spektrum der verfügbaren Methoden besprochen, angefangen von der herkömmlichen photoakustischen Detektion bis hin zum neuen photothermischen Laser-Probing und Frequenz-Multiplexing. Ihre Anwendung für die Messung von thermophysischen Wärmetransportparametern von Feststoffen wird dargelegt. Hierzu gehören Temperaturleitfähigkeit, Effusion, Wärmeleitfähigkeit und die spezifische Wärme. Es wird die Fähigkeit photothermischer Methoden hervorgehoben, eine breite Gruppe von Feststoffen, darunter Leiter- und Isolatormaterialien, Kristalle, geschichtete poröse und beschichtete Strukturen, dünne Filmschichten und inhomogene thermische Profile, thermisch zu untersuchen. Zuletzt werden spezielle Fähigkeiten der photothermischen Analyse, z.B. das Monitoring von thermodynamischen Oberflächenphenomänen und Phasenumwandlungsuntersuchungen, einschließlich von Hoch-T_c-Supraleitern, beschrieben, um einen vollständigen Überblick über das breite Leistungsfähigkeit der Methoden auf photothermischer Basis zu geben.